UDK 669.14:536.421.4
Original scientific article/Izvirni znanstveni članek

ISSN 1580-2949
MTAEC9, 48(4)537(2014)

MICROSTRUCTURE CHARACTERISTICS OF THE MODEL SPRING STEEL 51CrV4

ZNAČILNOSTI MIKROSTRUKTURE MODELNEGA VZMETNEGA JEKLA 51CrV4

Matjaž Torkar[1], Franc Tehovnik[1], Boštjan Arh[1], Monika Jenko[1], Božidar Šarler[2], Žarko Rajić[3]

[1]Institute of Metals and Technology, Lepi pot 11, 1000 Ljubljana, Slovenia
[2]Laboratory for Multiphase Processes, University of Nova Gorica, Slovenia
[3]CIMOS, d. d., Koper, Slovenia
matjaz.torkar@imt.si

Prejem rokopisa – received: 2014-01-28; sprejem za objavo – accepted for publication: 2014-04-03

There are many data on solidification processes in the literature, but there are no relevant comparisons performed for the formation of an as-cast microstructure, the formation of gas porosity, and the influence of different cooling rates on the solidification of the molten, non-killed spring steel 51CrV4. During a relatively rapid solidification the majority of the dissolved gases remain entrapped and due to a solid shell being formed they cannot escape from the steel. The result is the formation of gas porosity and a shrinkage cavity. Here we present the results of an investigation of the appearance and distribution of gas bubbles and a shrinkage cavity as well as the characterization of an as-cast microstructure in ingots of model spring steel, cast and cooled in different ways.

Keywords: spring steel, solidification, gas porosity, shrinkage cavity, SDAS, segregations

V literaturi je mnogo podatkov o procesu strjevanja, vendar pa ni podatkov o primerjavi med nastankom strjevalne strukture in nastankom poroznosti med strjevanjem nepomirjenega vzmetnega jekla 51CrV4. Pri relativno hitrem strjevanju večina raztopljenih plinov ostane ujetih v jeklu in zaradi nastanka skorje ne morejo pobegniti iz njega. Rezultat tega je nastanek plinske poroznosti in lunkerja. Predstavljeni so rezultati preiskav ter pojava in razporeditve plinskih mehurčkov in lunkerja, kot tudi karakterizacija mikrostrukture v ingotih vzmetnega jekla, ulitih in ohlajenih na različne načine.

Ključne besede: vzmetno jeklo, strjevanje, plinska poroznost, lunker, SDAS, izceje

1 INTRODUCTION

The typical stages of the solidification process in alloys can be described with the following stages: nucleation of a solid (stable nucleus); growth, which can be cellular or dendritic; solute distribution; and further growth, which proceeds by the movement of the interface and makes up the final as-solidified structure. The accumulation of the solute and the heat ahead of the interface can lead to conditions in which the liquid in front of the solidification front is supercooled. Under specific conditions the solidification becomes dendritic.

A characteristic tree-like structure of crystals growing along an energetically favourable crystallographic direction is called a dendrite in metallurgy. The form and the size of dendrites have a large influence on material properties.[1]

The requirement for dendrite formation is that the molten material is undercooled, below the freezing point of the solid. After the nucleation a spherical solid nucleus starts to grow as a sphere, later it becomes unstable and the solid shape depends on the preferred growth directions of the crystal. The anisotropy of the surface energy of the solid-liquid interface influences the growth direction. Besides that, the solidification rate influences the secondary dendrite arm spacing (SDAS), which can also be calculated using equation (1).[2]

The SDAS (λ) is a function of the cooling rate and can be written as:

$$\lambda = B \cdot \dot{T}^{-n} \tag{1}$$

where B and n are experimental constant parameters with values of 319.4 and 0.378, respectively,[3] and $\dot{T}$ is the cooling rate (°C/s) for this type of steel.

The SDAS (λ) can also be determined from a micrograph.[4]

During their grow dendrites bump into one another, until their growth is restricted by the other dendrites around them. At that point, the dendrite has reached its maximum size and it represents a grain. The space that exists between the grains is referred to as a grain boundary. If molten steel is cooled slowly, the result is the formation of a large grain size. However, when the steel is cooled quickly, the number of dendrites increases and a smaller grain size is the result.[5] All these parameters influence the microstructure development and the properties of the spring steel.[6]

Solidification proceeds at various rates. For that reason the microstructure is not homogeneous and variations in the composition appear as segregation. Segregation occurs because the diffusion in the solid phase is

too slow to achieve a uniform equilibrium structure, as predicted in the phase diagram. Segregation is classified, according to its scale, as macro-segregation or micro-segregation. This macro-segregation occurs on the scale of the grains or the entire casting and can be observed visually. It arises from a large-scale fluid caused by forced natural and solutal convection. The formation of segregation requires the transport of a solute-poor liquid and solid phases during the solidification over distances much larger than the dendrite arm spacing. The interdendritic flow of the liquid due to solidification shrinkage and changes in the liquid density are an unavoidable cause. These density changes can be caused by temperature changes or by changes in the composition of the liquid.[7–10]

It was revealed that the cooling rate also has an influence on the nucleation temperature and the width of the solidification interval.[11]

Micro-segregation usually arises between the dendrite arms. Due changes in the chemical composition, the strength and the ductility are lower in the transverse direction compared to the longitudinal axis of the dendrites.[12]

An important piece of data on the solidification structure is the coefficient of segregation k. It is determined as the rate of maximum and minimum concentration among the secondary dendrite arms ($k = C_{max}/C_{min}$) [13] or on the scale of the crystal grains.

Shrinkage cavities and voids are formed during the solidification due the volumetric shrinkage of the metal. This type of defect occurs because most metals contract by 2–6 % in terms of volume when the liquid transforms to a solid.[12] During hot rolling most of the voids are welded without any influence on the mechanical properties. In the case of gas bubbles (hydrogen), especially if they are close to the surface, they can form blisters on the surface during the cold rolling of sheets.[14]

Large shrinkage cavities can be minimized by the careful control of the heat transfer during the solidification process. For example, attaching a liquid metal reservoir, or riser, to a sand casting or to an ingot head, encourages shrinkage to occur in the riser, which feeds metal into the casting.

The molten metal dissolves and contains gases. The gases originate from the material, from the atmosphere or from reactions between the molten metal and the mould material. Since a liquid metal has a much higher solubility for gases than a solid metal, the gases are expelled during the solidification of steel. If they cannot escape they may form various defects in the material, e.g., porosity in the metal casting[15].

The maximum solubility of nitrogen in liquid iron is approximately $450 \cdot 10^{-6}$, and less than $10 \cdot 10^{-6}$ at ambient temperature (**Figure 1**).[16] The presence of the alloying elements in the liquid iron or steel affects the solubility of nitrogen. An important feature is that the presence of dissolved sulfur and oxygen limit the absorption of nitrogen because they are surface-active elements. This is exploited during steelmaking to avoid excessive nitrogen pickup, particularly during tapping.[16]

Shrinkage porosity is represented by small voids in a casting due to solidification shrinkage. Gas porosity is caused by gas bubbles that are evolved during the solidification and become trapped to form small, smooth, round voids or pinholes inside the casting.[17]

The bubbles can also be formed by a chemical reaction between the dissolved oxygen and the carbon in steel, to create carbon-monoxide bubbles. The carbon-oxygen reaction in Al-free steel can lead to blowholes, but also to pinholes in the cast material. Carbon and oxygen become enriched during the solidification in the interdendritic melt (as all elements), and the pressures of the carbon monoxide and carbon dioxide increase according to the reactions: [C] + [O] = {CO} and [C] + 2[O] = {CO_2}.

After the CO and CO_2 bubbles are initiated they start to grow with the advancing solid shell and form elongated blowholes.

During rapid solidification a majority of the dissolved gas remains entrapped, as due to the solid shell they cannot escape from the steel and this causes gas bubbles below the solidified shell during the solidification process. In the literature no comparisons are made from among the formation of gas porosity and the properties of the as-cast microstructure during the solidification of the molten spring steel 51CrV4 (1.8159) at different cooling rates. The standardized chemical composition of this type of steel is in mass fractions w(C) = 0.47–0.55 %, w(Si, max) = 0.4 %, w(Mn) = 0.7–1.1 %, w(P, max) = 0.025 % , w(S, max)) = 0.025 % , w(Cr) = 0.9–1.2 %, w(V) = 0.1–0.25 %.

The aim of the present investigation was to study the influence of the cooling rate of the not killed model spring steel on the appearance and distribution of the gas bubbles and the shrinkage cavity as well as the characterization of the as-cast microstructure.

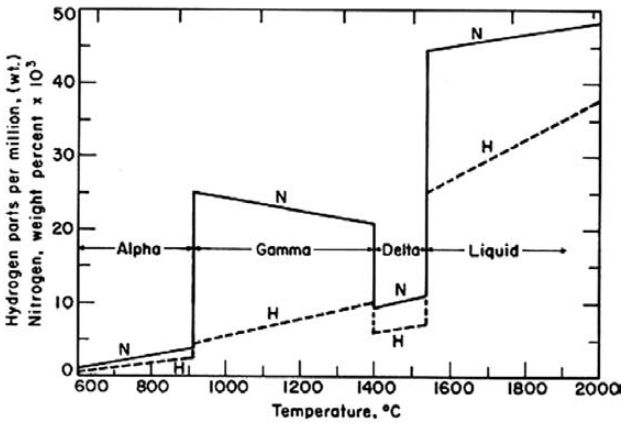

Figure 1: Solubility of nitrogen in iron for the temperatures 600–2000 °C[16]

Slika 1: Topnost dušika v železu pri temperaturah 600–2000 °C[16]

2 EXPERIMENTAL

The base material was prepared by the remelting of C, Si, Mn, Cr, V spring steel 51CrV4 in a Heraeus induction melting furnace. The final chemical composition of the experimental ingots was: w(C) = 0.53 %, w(Si) = 0.31 %, w(Mn) = 0,96 %, w(Cr) = 1.11 %, w(Mo) = 0.06 %, w(Ni) = 0.17 % and w(V) = 0.16 %. The melt was not deoxidized with Al prior to casting. The temperature of the melt in the melting furnace was 1580 °C. The melt was poured from the furnace into the preheated ceramic pot and then the melt with a temperature of 1530 °C was cast into an iron mould and sand form, to obtain different solidification cooling rates. The cross-section of the moulds and the sand cavity was 60 mm × 60 mm.

Special iron moulds were taken for the casting. The moulds consisted of two parts, separated by the diagonal cross-section, enabling the rapid opening and release of the ingot with a solidified shell. The thickness of the mould wall was 25 mm. The moulds were protected with a zirconium-oxide-based coating and heated prior to casting at 150 °C. The first sample, cast into an iron mould, was taken immediately after casting from the mould and cooled down in water. The second sample was cast into iron mould and cooled down in the mould. The third sample was cast and cooled down in a sand form. Three ingots were produced from the same melt, using three different cooling rates.

To characterize the soundness and the microstructure of the as-cast ingots, a 1-cm-thick plate was cut with a water-jet cutter, in a longitudinal direction, from all three ingots. Samples for metallography were cut from the plate in the middle of the ingots. The samples were prepared by a standard metallographic method and etched in Nital for observation in a light microscope.

Also, the individual micrographs were taken in 5 mm steps from the surface to the center of the ingots. The microstructure was observed using a Nikon Microphot FXA light microscope. The secondary dendrite arm spacing was determined from the etched samples. The microstructure was also observed with a JSM-6500F scanning electron microscope (SEM) equipped with a field-emission source of electrons and analysed with an INCA ENERGY Oxford Instruments Energy-Dispersive Spectroscopy (EDS).

3 RESULTS WITH DISCUSSION

The ingots solidified with three cooling rates were manufactured using the casting protocols as follows: a) cast in an iron mould and cooled in water, b) cast and cooled in an iron mould, c) cast and cooled in a sand form.

The ingot cooled in water was cut in a longitudinal direction, as presented in **Figure 2**. The cut was not very clear as the internal gas bubbles and shrinkage cavity (**Figure 3**) disturbed the high-pressure water-jet cutting process. A similar effect was also observed for the other two ingots, as presented in **Figures 4** and **5**.

The dendrites in the microstructure were observed only in the ingot cooled in water. The microstructure was martensitic. Normal crystal grains and no dendritic microstructure were observed in the other two ingots, where the microstructure was pearlite with a different inter lamellar spacing, dependent on the cooling rate. In the samples cooled in the mould or in sand some ferrite on the grain boundaries was observed near the surface of the ingot.

From the comparison of the longitudinal cross-sections of the ingots it is evident that there is a different formation and position of the gas bubbles and shrinkage porosity, both dependent on the cooling rate and the movement of the solidification front. In the ingot cooled

Figure 2: Longitudinal section of ingot cooled in water and cut with a high-pressure water jet cutter. The presence of gas bubbles disturbed the cutting process. The other two ingots were cut in the same way.

Slika 2: Vzdolžni prerez ingota, ohlajenega v vodi in razrezanega na rezalniku z visokotlačnim vodnim curkom. Tudi druga dva ingota sta bila razrezana na enak način.

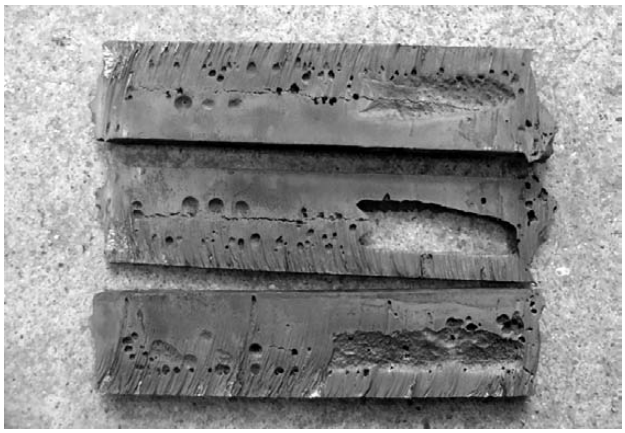

Figure 3: Longitudinal section of ingot, cooled in water. Observed are the gas bubbles and the closed shrinkage cavity in the head and the longitudinal central crack due to rapid cooling after solidification. Evident is the thickness of the solidified shell prior to cooling in the water. All the gas bubbles are below this shell.

Slika 3: Vzdolžni prerez ingota, ohlajenega v vodi, s plinskimi mehurčki in zaprto poroznostjo v glavi ter vzdolžna razpoka v sredini zaradi hitrega ohlajanja po strjevanju. Vidna je debelina strjene skorje pred ohlajanjem v vodi. Vsi plinski mehurčki so pod to skorjo.

Figure 4: Longitudinal section of ingot cooled in iron mould. Gas bubbles and small closed shrinkage cavity moved toward the head. The solidification front moves toward the head, so the gas bubbles are concentrated below the head, where the last melt solidified.

Slika 4: Vzdolžni prerez ingota, ohlajenega v železni kokili. Plinski mehurčki in majhna zaprta poroznost so pomaknjeni bliže h glavi. Fronta strjevanja se je pomikala proti glavi, zato so plinski mehurčki koncentrirani pod glavo ingota, kjer se je strdila zadnja talina.

in water larger gas bubbles and a large shrinkage cavity was observed, as well as a long crack in the middle of the ingot's longitudinal direction. Evident is also the thickness of the rapidly solidified shell that pushed the bubbles away (**Figure 3**)

The relatively sound material, concerning gas bubbles, is in the ingot cooled in the iron mould. Some gas bubbles are in the central part of the ingot, closer to the head. The reason is the solidification front that moved from the sides and from the bottom toward the head of ingot, where the gas bubbles and the shrinkage porosity are collected (**Figure 4**).

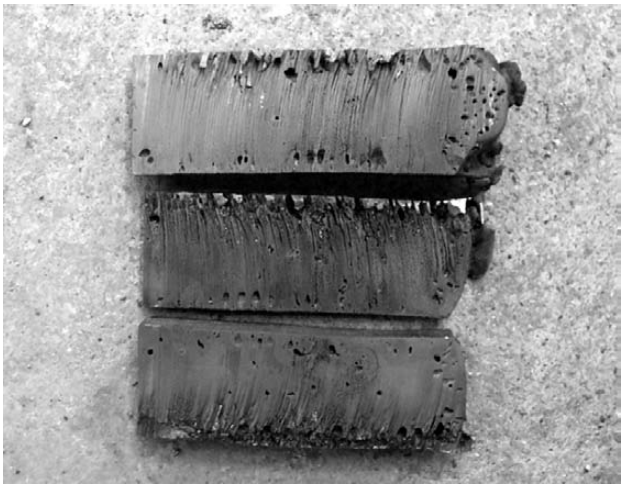

Figure 5: Longitudinal section of ingot, cast and cooled in sand form. Due to the lower solidification rate, the growth of the shell was slower and the bubbles are closer to the surface. No shrinkage cavity is observed.

Slika 5: Vzdolžni prerez ingota, ulitega in ohlajenega v pesku. Zaradi počasnejšega ohlajanja je bila počasnejša tudi rast skorje in iz taline izločeni mehurčki so bližje površini. Lunkerja ni opaziti.

Almost no shrinkage porosity is observed in the ingot cast and cooled in the sand form (**Figure 5**). The gas bubbles (pinholes) are present along the whole ingot and closer to the surface, as the movement of the solidification front was slower. Some individual pinholes are also present in the central part of ingot and more numerous gas bubbles are closer to the head of the ingot.

In general, the gas bubbles and shrinkage porosity for the present steel are more expressed than the steel melt that was not killed with Al or other desoxidant. For that reason the gas content in the melt was higher and as a consequence also the number of bubbles was higher.

It is evident that the dissolved gases (**Figure 1**) did not have enough time to separate completely from the melt, due to the relatively high cooling rate, and the small cross-section at all three ingots. The concentration of gas bubbles depends on the cooling rate. A large closed shrinkage cavity in the head and larger gas bubbles below the surface were observed in the ingot with the fastest solidification rate. In the ingot cooled in the mould the bubbles and the shrinkage cavity moved toward the head of the ingot.

For the ingot cooled in the sand form most of the gas bubbles were observed closer to the surface and no shrinkage cavity was observed in the head of the ingot. This is also evidence that the melt was not killed with aluminium or silicon.

The samples for metallography were prepared from plates cut with a water jet from ingots. Light microscopy revealed that the ingot with the fastest cooling in water has a dendritic microstructure with martensite (**Figure 6**) and visible interdendritic segregations.

The other two ingots, with the slower cooling rate, have a perlitic microstructure with crystal grains of different size and also different interlamelar spacings of cementite lamelas in pearlite (**Figure 7**). The slower cooling rate enables a pearlite transformation in the material.

Due to the relatively slow solidification and cooling in the iron mould and in the sand form, the segregations are clearly visible for the ingot cooled in water. The dendrite arm spacing (**Table 1**) was determined either by measurements of the segregation distance or calculated using equation (1). The cooling rate was also calculated using equation (1).

Table 1: Secondary dendrite arm spacing λ, measured and determined with equation (1), for three cooling rates of the ingots

Tabela 1: Oddaljenost sekundarnih dendritnih vej λ, izmerjena in določena z enačbo (1), za tri hitrosti ohlajanja ingotov

Parameter	Cooling of ingot		
	Water (μm)	Iron mold (μm)	Sand form (μm)
Measured SDAS, λ/μm	50	150	170
Calculated SDAS, λ/μm	52	182	210
Calculated T/(°C/s)	121.7	4.4	3.0

λ – secondary dendrite arms spacings (SDAS)
T – cooling rate

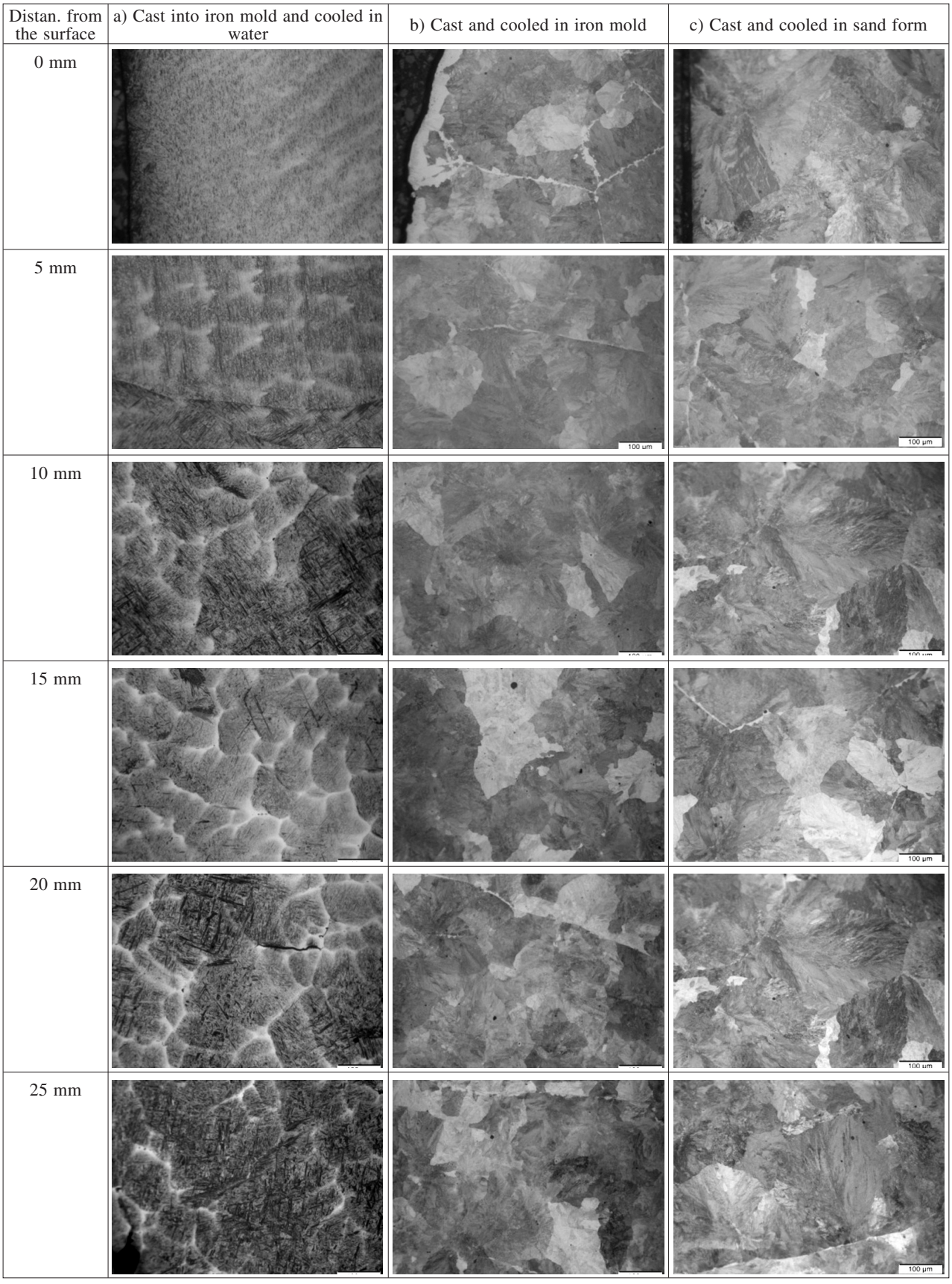

Figure 6: Comparison of as-cast microstructure of ingots at given distances from the surface. Light microscope (magnification 100-times).
Slika 6: Primerjava mikrostrukture ulitih ingotov pri dani razdalji od površine. Svetlobni mikroskop (povečava 100-kratna).

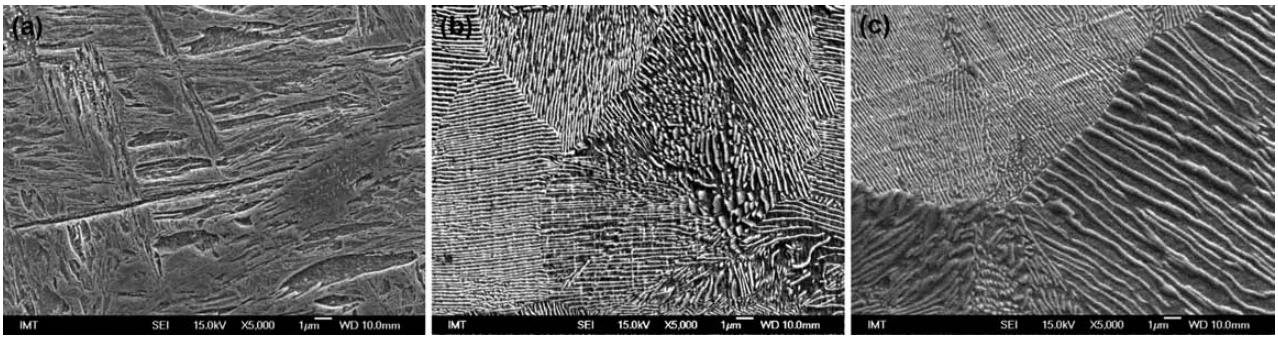

Figure 7: Microstructure of ingots: a) cooled in water, b) cooled in iron mould and c) cooled in sand, (SEM)
Slika 7: Mikrostruktura ingotov: a) ohlajanje v vodi, b) ohlajanje v železni kokili in c) ohlajanje v formi iz peska (SEM)

From the results given in **Table 1** it is clear that the highest cooling rate was in the ingot cooled in water. As can be seen from **Figures 6a** and **7a** the obtained microstructure under the light microscope was martensite for the ingot cooled in water. On the other hand, the cooling rates of other two ingots, solidified in the iron mould and in the sand, are smaller, which is also confirmed by the microstructure (**Figures 6b**, **6c**, **7b** and **7c**). The microstructures of the ingot solidified in the iron mould and in the sand are pearlite. The reason is in the formation of a gap in the iron mould that prevents faster cooling. The lowest cooling rate is, as expected, in the sand form. The ratio of the cooling rates, compared to the cooling rate in the sand are: 40.56 : 1.46 : 1.00. It means the cooling rate of the ingot in the water was 40.56 times faster compared with the cooling rate of the ingot in the sand form. The cooling rate also influences the SDAS. The secondary dendrite arm spacing, compared to the cooling rates in water, are 1.00 : 3.5 : 4.03. The SDAS is 4.03 times larger in the ingot that was cast and cooled in the sand form, compared to the ingot that was cooled in water.

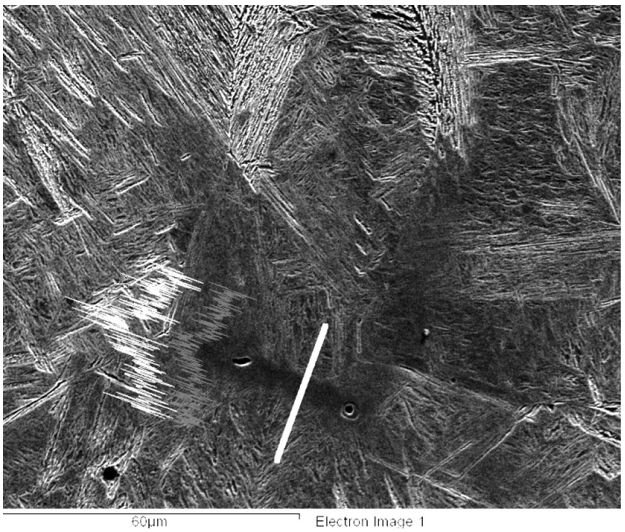

Figure 8: Segregation of chromium and vanadium along the line for ingot cooled in water (SEM)
Slika 8: Izceja kroma in vanadija vzdolž črte v ingotu, ohlajenem v vodi (SEM)

The measurements of the Cr segregations in all three ingots revealed larger differences in the Cr and V concentrations only in the material cooled in water (**Figure 8** and **Table 2**) and less expressed segregations of Cr in ingots cooled in the mould or in the sand (**Tables 3** and **4**), because of the lower cooling rate.

A less expressed segregation of V was observed only in an ingot cooled in water. In the other two ingots the segregation of V was not detected. For that reason only a comparison of the Cr segregations in all three ingots is presented (**Tables 2**, **3** and **4**).

Table 2: Segregations of Cr in the ingot cooled in water
Tabela 2: Izceje Cr v ingotu, ohlajenem v vodi

	w(Cr)/%	$k = C_{max}/C_{min}$
Centre of Dendrite 1	1.42	
Between dendrite 1/2	1.83	1.28
Centre of Dendrite 2	1.00	
Between dendrite 2/3	1.34	1.34
Centre of dendrite 3	1.42	
Between dendrite 3/4	1.75	1.23

Table 3: Segregations of Cr in the ingot cooled in the mould
Tabela 3: Izceje Cr v ingotu, ohlajenem v kokili

	w(Cr)/%	$k = C_{max}/C_{min}$
Centre of Dendrite 1	1.13	
Between dendrite 1/2	1.20	1.06
Centre of Dendrite 2	1.20	
Between dendrite 2/3	1.51	1.25
Centre of dendrite 3	1.27	
Between dendrite 3/4	1.33	1.04

Table 4: Segregations of Cr in the ingot cooled in sand
Tabela 4: Izceje kroma v ingotu, ohlajenem v pesku

	w(Cr)/%	$k = C_{max}/C_{min}$
Centre of Dendrite 1	1.20	
Between dendrite 1/2	1.22	1.01
Centre of Dendrite 2	1.20	
Between dendrite 2/3	1.28	1.06
Centre of dendrite 3	1.22	
Between dendrite 3/4	1.26	1.03

The experiments revealed that the increased cooling rate decreases the secondary dendrite arm spacing,

increases the intensity of the segregation of Cr and influences the formation and distribution of gas bubbles and the shrinkage cavity in as-cast material.

For the further processing of the steel the gas bubbles may not be so detrimental because they can be welded during a hot deformation.

To decrease the quantity of gas bubbles, the steel melt needs to be killed more intensively, prior to casting.

4 CONCLUSIONS

Based on the investigations on as-cast 60 mm × 60 mm not-killed spring steel 51CrV4 ingots, the following conclusions can be drawn.

- A comparison of the as-cast microstructures of experimental cast ingots revealed the dendritic structure only in an ingot cooled in water.
- The ingot cooled in water had a martensitic microstructure.
- The ingots cooled in an iron mould or in a sand form have a similar microstructure with pearlite grains, which were coarser for the cooling in the sand form. No dendrites were observed. The slower cooling rate enabled the formation of pearlite with ferrite on some grain boundaries.
- The increased cooling rate decreases the secondary dendrite arm spacing and also influences the formation, as well as the layout, of the gas bubbles and the shrinkage cavity in as-cast spring steel.
- A slower cooling rate caused the formation of gas bubbles closer to the surface of the as-cast ingot.
- In the ingot cooled in water larger gas bubbles were observed, distributed across the whole ingot. A large shrinkage cavity was present, as well as longitudinal cracks in the middle of the ingot.
- The increased cooling rate also increases the segregation of chromium.
- To decrease the quantity of gas bubbles, the steel needs to be aluminium or silicon killed more intensively, prior to the casting.

Acknowledgement

Authors wish to thank to Slovenian Research Agency for the financial support in the frame of projects No. L2-3651 and P2-0132.

5 REFERENCES

[1] W. Kurz, D. J. Fisher, Fundamentals of Solidification, 4th ed., Trans Tech Publ. Ltd, Switzerland 1998

[2] T. W. Clyne, W. Kurz: Metall. Trans. A, 12 (**1981**), 965–71

[3] http://steeluniversity.org

[4] J. Campbell, Castings, Butterworth-Heinemann, 2003, 270

[5] H. Fredriksson Hasse, U. Akerlind, Solidification and crystallization processing in metals and alloys, John Willey and sons, 2012

[6] B. Podgornik, V. Leskovšek, M. Godec, B. Senčič, Microstructure refinement and its effect on properties of spring steel, Materials Science and Engineering A, 599 (**2014**), 81–86

[7] M. C. Flemings, G. E. Nereo, Trans. TMS-AIME, 239 (**1967**), 1449–61

[8] R. Mehrabian, M. Keane, M. C. Flemings, Metall. Trans., 1 (**1970**), 1209–20

[9] T. Fuji, D. R. Poirier, M. C. Flemings, Metall. Trans. B, 10 (**1979**), 331–39

[10] Y. M. Won, B. G. Thomas, Simple Model of Microsegregation during Solidification of Steels, Metallurgical and Materials Transactions A, 32 (**2001**), 1755

[11] D. Steiner Petrovič, M. Pirnat, G. Klančnik, P. Mrvar, J. Medved, The effect of cooling rate on the solidification and microstructure evolution in duplex stainless steel, J. Therm. Anal. Calorim., 109 (**2012**) 3, 1185–1191

[12] K. O. Yu (ed.), Modeling for Casting and Solidification Processing, 1st ed., CRC Press, 2001, 12

[13] M. Torkar, B. Šuštaršič, Preiskava vodno atomiziranega prahu iz zlitine Nimonic 80 A, Kovine zlitine tehnologije, 26 (**1992**) 1–2, 100–103

[14] H. J. Grabke, Supersaturation of iron with nitrogen, hydrogen or carbon and the consequences, Mater. Tehnol., 38 (**2004**) 5, 211–222

[15] P. S. Wei, C. C. Huang, Z. P. Wang, K. Y. Chen, C. H. Lin, Growths of bubble/pore sizes in solid during solidification – an in situ measurement and analysis, Journal of Crystal Growth, 270 (**2004**) 3–4, 662–673

[16] http://www.keytometals.com

[17] R. A. Stoeh, Modeling the influence of fluid flow on the development of porosity and microstructure in castings, Canadian Metallurgical Quarterly, 37 (**1998**) 3–4, 179–184